Faults Identification in Wind Turbines' Transformers

Daniela Caetano Alves

Instituto Superior Técnico, Lisboa, Portugal

The transformer is one of the main electrical equipment in electrical systems and in particular in wind generation systems. From the financial point of view, companies have been taking a more preventive action to minimize the effect of transformer failures in the system and to reduce the maintenance cost of this equipment. In this context, the detection of incipient failures is imperative in order to reduce the damage it may suffer. This requires continuous monitoring and diagnostics of the transformer status, minimizing damage associated with equipment defects. This paper presents a review of the main causes of transformer failures and the methodologies for fault diagnosis. Two transformer models for fault simulation are developed, an analytical model and a finite element model. These models are used as a diagnostic tool for faults between turns and in the diagnosis of the insulation resistance aging. For the diagnosis of failures between turns comes the analysis of the magnetization current. In this diagnosis, short circuit events between consecutive turns and non-consecutive turns are performed. The other diagnosis tool is based on the detection of aging of the insulation resistance by analyzing the leakage current detection for each resistance value tested.

Keywords— Detection, Diagnostics Models, Failures, Transformer

I. Introduction

Electricity is a sector that has changed significantly in recent times, moving from a standard vertical sector to a horizontal hierarchy. The cessation of regulated monopolies and the adhesion of market mechanisms in some sectors of activity have caused strong competitiveness at a global level resulting in lower energy costs. In this context, leading companies are the ones ensuring a more qualified and reliable service. On the other hand, the emergence of data processing techniques, such as machine learning and deep learning, have added value to the data typically acquired by companies in this sector.

The renewable sector, namely wind power, is a relevant sector in this age of data science and energy transformation. Today's available resources make it possible to anticipate operational problems and keep turbines in good yield. However, although these technologies have strengths, they also hold some weaknesses. In the specific case of this work the focus will be on transformers, as this device proves to be particularly problematic due to its capital and maintenance cost. High costs are often accompanied by the increase of the cost of raw materials (copper) as well as high demand for emerging economies. For these reasons, companies are forced to postpone the replacement or renewal of this equipment, that means that further malfunctions, which often result in considerable damage to companies, are prone to occur.

In order to solve the problems described, companies have been adopting maintenance strategies. The implementation of a maintenance strategy relies on the development of diagnostic methods that enable the identification of incipient transformer failures to avoid high repair costs or even service failures. This covers non-disruptive methods, so-called online methods as well as offline diagnostic methods.

The proposed work will address the identification of transformer winding faults and insolation aging through simulations with analytical and finite element models, in order to create profiles for each type of fault. This data will be essential for maintenance diagnostics, which will contribute to the reduction of failures between windings. Another relevant aspect of the study is the computational time analysis of the developed models, since the data treatment to identify a fault should be done in a timely manner.

II. Short Circuit Modeling Between Turns In The Transformer

A. Analytical model of the transformer

The analytical model of the transformer is based on the Ampère and Induction laws applied to transformer, Fig 1. First off, by applying a voltage at the ends of the primary windings of each phase, by the Induction Law (1), a variation in the phase magnetic flux will occur.

$$\begin{cases} u_{1a} = r_{1a} i_{1a} + \dfrac{\partial \Psi_{1a}}{dt} \\ u_{1b} = r_{1b} i_{1b} + \dfrac{\partial \Psi_{1b}}{dt} \\ u_{1c} = r_{1c} i_{1c} + \dfrac{\partial \Psi_{1c}}{dt} \end{cases} \quad (1)$$

The secondary of the transformer is terminated by a resistive load, r_L. Using the Induction law, now for the secondary windings of the transformer, results in the equation system in eq. (2).

$$\begin{cases} \mathrm{i_{2a}} = -\dfrac{\partial \Psi_{2a}}{\mathrm{dt}} \dfrac{1}{\mathrm{r_L} + \mathrm{r_{2a}}} \\ \mathrm{i_{2b}} = -\dfrac{\partial \Psi_{2b}}{\mathrm{dt}} \dfrac{1}{\mathrm{r_L} + \mathrm{r_{2b}}} \\ \mathrm{i_{2c}} = -\dfrac{\partial \Psi_{2c}}{\mathrm{dt}} \dfrac{1}{\mathrm{r_L} + \mathrm{r_{2c}}} \end{cases} \quad (2)$$

In order to link secondary currents with primary magnetic fluxes, the relationship between primary and secondary magnetic linkage fluxes must be introduced: $\Psi = N\,\phi$.

Since the magnetic flux is the relationship between the magnetic flux density and the chosen section area, it is possible to obtain the value of the magnetic flux density, B, from the magnetic fluxes. The linkage flux expresses a relation between the number of turns and the magnetic core flux, $\Psi = N\,\phi$. From these two equations, a third one (3), which correlates the connected fluxes with B, is presented.

$$B_i = \frac{\Psi_i}{N_i S} \tag{3}$$

By obtaining the values of the magnetic flux density, B, and using the B(H) curve of the FeSi material we can determine the magnetic field strength, H, to a certain applied primary voltage value. In this way, the achieved magnetic field strength is determined by the value of the applied magnetic flux density, Fig. 2.

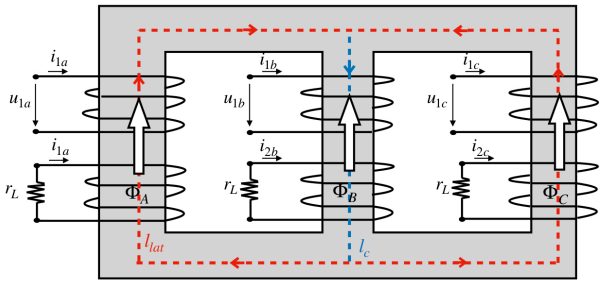

Figure 1 - Application of Ampère Law and Induction Law

The relationship between the electric current and the intensity of the magnetic field can be obtained through the Ampère Law (4), applied to one closed paths drawn in Figure 1. Equation (4) associates the line integral of the magnetic field intensity vector $\boldsymbol{H}$ along a closed path l to the total current involved in that path. The central section has length l_c and the lateral sections have l_{lat} length.

$$\oint_l \vec{H}\,\vec{dl} = \int_S \vec{J}\,\vec{n}\;dS \tag{4}$$

Equation (6) refers to Kirchhoff's law, which combined with the system of equations (5) gives the relation between the magnetic field and magnetic flux density with the primary and secondary currents.

$$\begin{cases} H_A\,l_{lat} - H_B\,l_c = N_1\,i_{1a} + N_2\,i_{2a} - (N_1\,i_{1b} + N_2\,i_{2b}) \\ H_C\,l_{lat} - H_B\,l_c = N_1\,i_{1c} + N_2\,i_{2c} - (N_1\,i_{1b} + N_2\,i_{2b}) \end{cases} \tag{5}$$

$$\phi_A + \phi_B + \phi_C = 0 \tag{6}$$

The transformer's analytical model was implemented in a SIMULINK environment. The scheme can be observed in Figure 2.

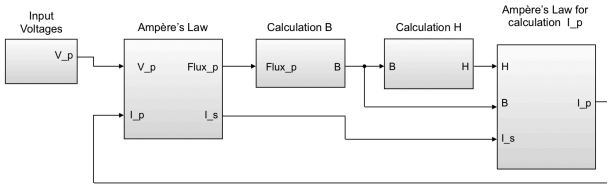

Figure 2 - Analytical analysis scheme.

1) Short circuit between consecutive turns

The method presented here simulates a short circuit between consecutive turns, which in practice corresponds to the grouping of these turns, thus contributing to the reduction of the number of turns compared to the initial number. In order to simulate short circuits between consecutive turns, the number of turns in the last block of Figure 2 is reduced, that is, the winding to be displayed for the short circuit is included by adding the defect percentage.

2) Short circuit between non-consecutive turns

This second method of shorting between turns differs from the first since the shorting is not consecutive, which means there is a shorting in two turns that touch each other but the turns between them are not shorted. The analytical model of this method was elaborated in Simulink environment, Figure 3.

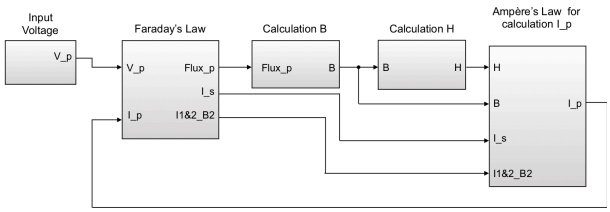

Figure 3 - Non-consecutive turns short circuit model

In this model, the defect phase (phase b) was reconstructed in relation to the previous model, keeping the same equations as for phases a and c. In Figure 4 shows the electrical circuit that defines the fault phase in the primary transformer winding.

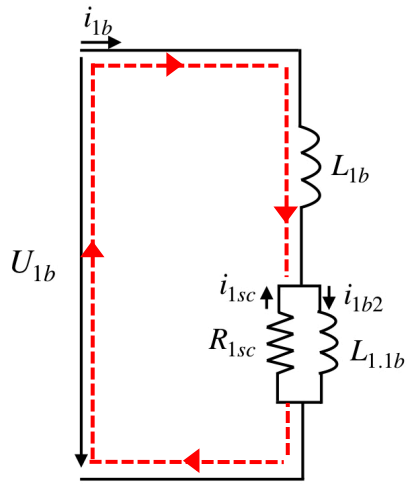

Figure 4 - Non-consecutive turns short circuit model

Coil L_{1b} has a resistance $R_{coil} \times (1 - f_p)$ where f_p represents the percentage of shorted turns of the primary winding. And the coil $L_{1.1b}$ also has a resistance, $R_{coil} \times f_p$.

Applying the Law of Induction to the mesh represented in red, Figure 4, comes

$$u_{1b} = \left[R_1 + R_{coil} \times \left(1 - f_p\right)\right] i_{1b} + R_{coil} \times f_p \times i_{1b2} + \frac{\partial \Psi_{1b}}{\partial t} \quad (7)$$

Integrating (7) removes the value of the flow,

$$\Psi_{1b} = \int u_{1b} - \left[R_1 + R_{coil} \times (1 - f_p)\right] + R_{coil} \times f_p \times i_{1b2} \quad (8)$$

Applying the Induction Law to the short circuit loop (LC circuit),

$$0 = i_{1b2} \times R_{coil} \times f_p + i_{1sc} \times R_{sc} + \frac{\partial \Psi_{1sc}}{\partial t} \quad (9)$$

The flow Ψ_{1sc} can be written by the relation, $\Psi_{1sc} = f_p \, \Psi_{1b}$ and from (9) the current flowing through the coil is $L_{1.1b}$ calculated.

$$i_{1b2} = -\frac{1}{R_{coil} \times f_p} \left[i_{1sc} \times R_{sc} + f_p \times \frac{\partial \Psi_{1b}}{\partial t}\right] \quad (10)$$

Applying Kirchhoff's Law (11) to the circuit, the values of all the present currents of the fault phase circuit are determined.

$$i_{1sc} = i_{1b2} - i_{1b} \quad (11)$$

Also in the secondary winding changes were made in the defect phase equations. In Figure 5 shows the wiring diagram for the secondary phase failure phase.

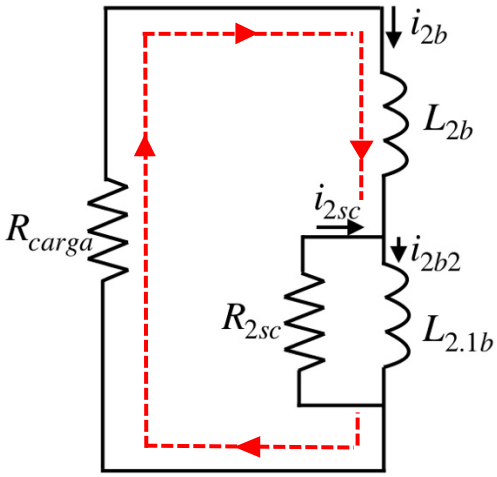

Figure 5 – Eletrical phase b circuit of secondary winding

Following the same procedure for secondary winding, the General Induction Law (12) was applied to the mesh represented in red in Figure 5.

$$i_{2b2} \left[R_{load} + R_{coil} \times (1 - f_s)\right] + i_{2b2} \times R_{coil} \times f_s + \frac{\partial \Psi_{2b}}{\partial t} = 0 \quad (12)$$

The relationship between secondary winding flow and primary winding flow is described by equality,

$$\Psi_{2b} = \Psi_{1b} \frac{N_{2b}}{N_{1b}} \quad (13)$$

$$i_{2b2} \left[R_{bobina} \times f_s + i_{2sc} \times (1 - f_s)\right] + i_{2b2} \times R_{2sc} + f_s \times \frac{\partial \Psi_{2b}}{\partial t} = 0 \quad (14)$$

By the Law of Nodes, the values of the current that travel the electrical circuit are determined (Figure 5).

$$i_{2sc} = i_{2b2} - i_{2b} \quad (15)$$

Finally, the Ampère's Law was defined in order to obtain the currents in the primary winding.

$$\begin{cases} H_a l_{lat} - H_b l_c = N_{1a} i_{1a} + N_{2a} i_{2a} \\ -\left[N_{1b}(1 - f_p) i_{1b} + N_{1b}(f_p) i_{1b2}\right] - \\ \left[N_{2b}(1 - f_s) i_{2b} + N_{2b}(f_s) i_{2b2}\right] \\ \\ H_c l_{lat} - H_b l_c = N_{1c} i_{1c} + N_{2c} i_{2c} - \\ \left[N_{1b}(1 - f_p) i_{1b} + N_{1b}(f_p) i_{1b2}\right] - \\ \left[N_{2b}(1 - f_s) i_{2b} + N_{2b}(f_s) i_{2b2}\right] \end{cases} \quad (16)$$

$$B_a + B_b + B_c = 0 \quad (17)$$

In order to solve the equation, we added the Law of Nodes with magnetic field density and passed to a matrix system that was defined in a Matlab file.

B. Finite Element Model (FEM)

The FEM model is based on the division of the system into small elements (finite elements) where fields are defined based on base functions (linear, quadratic, cubic, etc.) and with associated weights. These elements are associated, creating a system of equations. These equations, in turn, lead to the construction of a matrix system that correspond to the system's physical equations (Ampère and Induction Laws) and in which the solution is numerical.

For the description of the transformer's finite element model and the failures associated with the short circuit between turns, the following are presented: 1) the transformer geometry, 2) the electromagnetic characteristics of the materials used and the simulation parameters, 3) the associated physical equations and 4) the discretization mesh used.

1) Geometry Description

The geometry adopted for the transformer is shown in Figure 6. The transformer was designed for a nominal voltage of 10 kV (phase-to-phase) and a rated power of 10MVA, at a frequency of 50 Hz.

The magnetic core is formed by two horizontal columns and three equal and symmetrical vertical columns. Horizontal columns have a rectangular section $w_{c\_lat} \times h_{c\_lat}$ and vertical columns also have a rectangular section $w_{c\_ver} \times h_{c\_ver}$. The primary and secondary windings are distributed over the three vertical columns, corresponding to phases a, b and c, respectively. Each winding occupies an area of value $w_{Cu} \times h_{Cu}$. Each winding was designed with 263 turns, each one with six conductors in parallel (total number of turns is 1700).

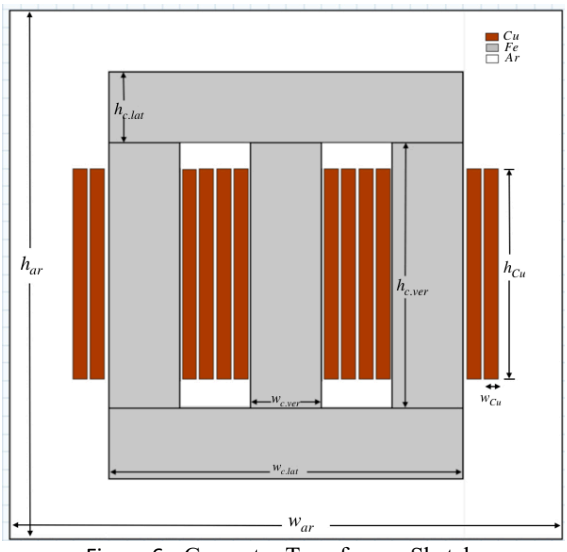

Figure 6 - Geometry Transformer Sketch

2) Global Materials and Parameters

The materials used in the construction of the simulation model were a) air, b) copper (Cu) and c) Laminated Silicon-Iron (FeSi).

- Air is characterized by zero electrical conductivity, 0 [S/m], permittivity (ε_r) and unit relative magnetic permeability (μ_r).
- The copper used for the transformer windings is defined by an electrical resistivity of 1.667×10^{-8} [Ωm] and a magnetic permeability (μ_r) of value 1.
- Laminated Silicon Iron is the material that forms the core of the transformer. The nonlinear B(H) curve is presented in Figure 7.

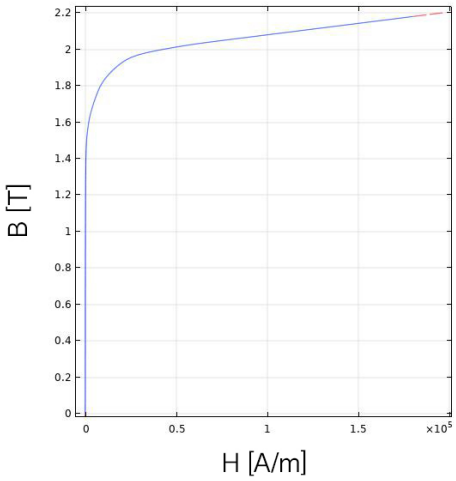

Figure 7 - B(H) Curve of the iron core

The core construction consists on a stack of laminated silicon iron, insulated between them. This material has an anisotropic electrical conductivity where the x and y axes have a conductivity of 1.69×10^6 S/m and the z axis a negligible conductivity. The value of the z axis conductivity depends on the sheet lamination thickness, sheet d_{sheet} and the height of the magnetic circuit, column h_{column}.

$$\sigma_z = \left(\frac{d_{sheet}}{h_{column}}\right)^2 \sigma_x$$

3) Physical Equations

a) Magnetic Field Equations

Magnetic field equations are used to describe the magnetic behavior of each material, considering the 2D geometry of the problem. The physical equations defined in this section are the Ampere Law, (18), the Induction Law, (19) and the properties of the medium, (20). For the medium equations the properties of the materials described above are used. In addition to these equations, boundary conditions are required, which in this case correspond to those of magnetic isolation applied to the outer limits of the problem.

The source of the problem is the current density applied to each of the windings, J_{ext}, but this imposition is not done directly but by applying voltage to the winding terminals. The

relationship between the applied voltage and the originated current density is made through the use of an additional electric circuit in which the windings are represented by a model in concentrated parameters.

$$\nabla \times H = J \tag{18}$$

$$B = \nabla \times A \qquad E = -\frac{\partial A}{\partial t} \tag{19}$$

$$J = \sigma E, \qquad B = f(H) \tag{20}$$

b) Eletric Circuit Diagram

An electrical circuit was used to relate the voltages applied to the windings and the currents that originate in them, Figure 8. The electrical circuit of the transformer is described by concentrated parameters that represent physical quantities. R1, R2 and R3 represent the resistances of each phase of the primary winding, respectively, and V1, V2 and V3 correspond to the voltages imposed on the primary winding. The transformer is simulated by applying sinusoidal alternating voltages to the primary windings and with a three-phase resistive load to adjust the secondary current to its rated value. The induction coefficients of the primary windings are determined by the FEM magnetic field model which, through an iterative process, will converge the solutions of the transformer's electric and magnetic circuits. Note that the phase b windings are divided into 3 in order to facilitate the simulation of short circuits between turns, between points 7 and 8 or 11 and 13.

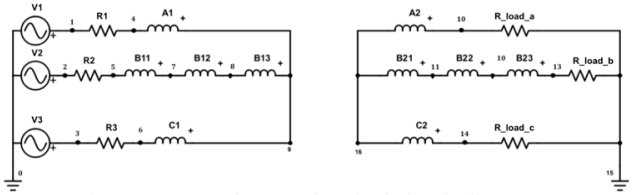

Figure 8 - Transformer electrical circuit diagram

c) Discretization Mesh

The finite element method divides the model into small elements of geometrically simple shapes, in this case triangles, forming a mesh. In each triangle, a set of polynomial functions, called base functions, is used to approximate the structural displacement field (how much the object deforms in each of the three coordinate directions). The dimensions of the elements of this mesh determine the accuracy of the final solution. The smaller the size of the mesh elements, the greater the accuracy of the problem solution, but also the longer its computation time. In this case, as the transformer geometry contains small spaces between the windings, a finer mesh was defined in the zones represented in blue (Figure 9) in order to obtain a more accurate result in these zones, while maintaining the acceptable overall computation time.

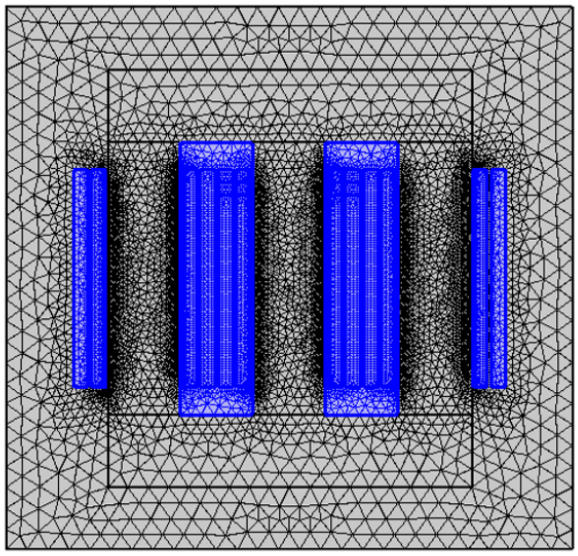

Figure 9 - Descripting mesh representation

III. RESULTS

Results presented are based on the simulation of the defective transformer through the use of analytical models and finite element models. On the one hand, finite element analysis enables detailed results to be obtained throughout the transformer, the higher its accuracy being, but in contrast, its computation time is much longer than that of analytical models. On the other hand, the developed analytical model needs a much shorter computation time than the previous model, but due to the use of approximations, its accuracy is lower.

A. Short circuit between consecutive turns

The short circuit simulation between consecutive turns was performed by changing the number of effective turns of the transformer. Simulations were performed for various reductions in the number of turns (1%, 2%, 3% and 5%) of the primary winding in phase b.

1) Primary side short-circuit

Figure 10 and Figure 11 illustrate the evolution of primary and secondary currents, respectively, in the case of a 3% reduction in the number of turns of the primary winding for finite element analysis. Shorting between consecutive turns of the primary winding causes an increase in the input phase of the affected phase, resulting in a current unbalance system. In this type of fault, the secondary winding, Figure 9, undergoes changes, also causing an increase in current in the same fault phase.

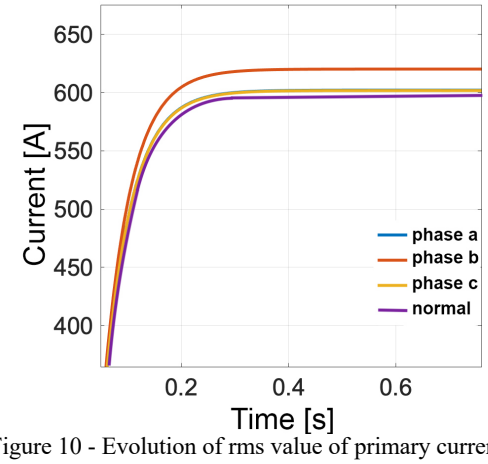

Figure 10 - Evolution of rms value of primary current

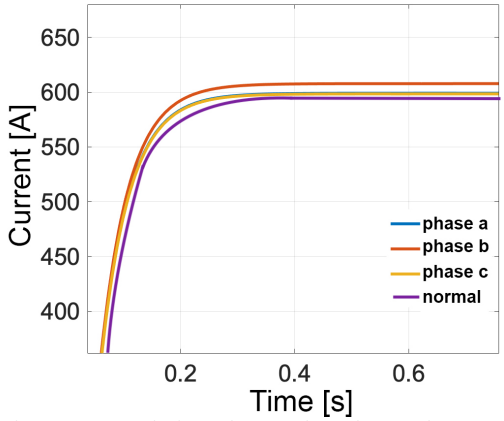

Figure 11 - Evolution of rms value of secondary current

From the point of view of magnetization currents, it is possible to identify the defect and its phase, even with only 1% of defect, and this effect is similar in both models. The method suggested in the previous chapters states that this current should be between 0.1% -0.3% of the nominal current value (Fofana, 2018). Analyzing Table 1 shows that only with 1% of the turns short circuit the magnetization current violates the established condition.

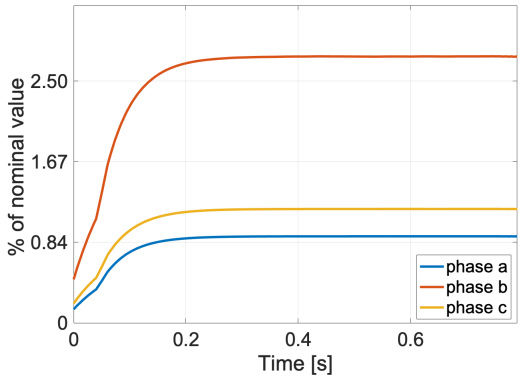

Figure 12 - Evolution of the rms value of the magnetization current

Table 1 – Primary side short circuit magnetization current

	1%	2%	3%	5%
Phase a	0,4% I_N	2,1% I_N	4,7% I_N	11,9% I_N
Phase b	1,1% I_N	4,4% I_N	9,8% I_N	24,1% I_N
Phase c	0,7% I_N	2,4% I_N	5,0% I_N	12,2% I_N

2) Secondary side short circuit

Figure 13 and Figure 14 show the primary and secondary currents respectively when a short circuit occurs in the secondary winding.

A fault in phase *b* of the secondary winding leads in both analyzes to a reduction in the current from the secondary side and also on the primary side in the phase in which the defect occurs. This is because the number of effective turns in the secondary decreases. By decreasing, the induced secondary voltage decreases and, since the transformer load is a pure resistance, the current could also reduce to the phase in which the fault occurs. This effect of the current reduction is most evident in the finite element model, being visible in all cases presented, while in the analytical model only becomes visible after 3% of defect. Input voltages do not change from nominal value.

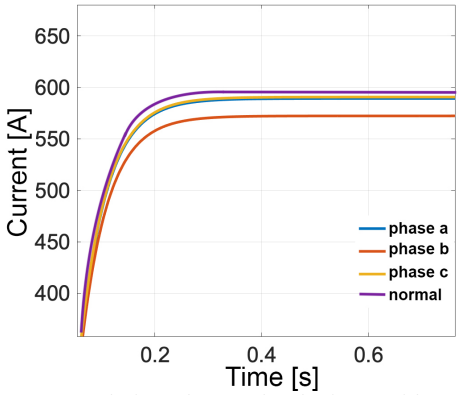

Figure 13 - Evolution of rms vale of primary side current

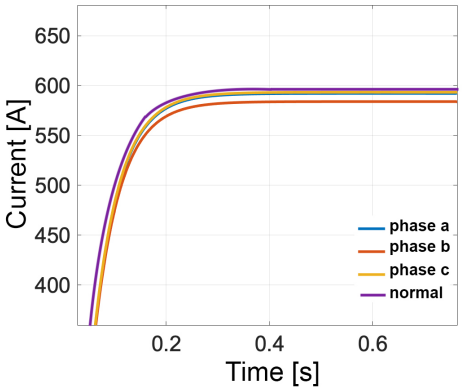

Figure 14 - Evolution of rms value of secondary side current

The magnetization current, Figure 15 show a larger increase in the fault phase compared to the other two phases. We can verify through Table 2 the percentage values in relation to the nominal value. It is quickly seen that for one percent of shorted turns, the condition of the magnetization

current in the range 0.1% -0.3% of the nominal value is not met.

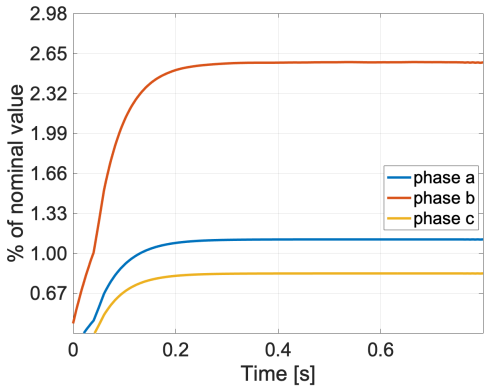

Figure 15 - Evolution of rms valuer of magnetization current

Table 2 – Secondary side short circuit magnetization current

	1%	2%	3%	5%
Phase a	0,4% I_N	2,1% I_N	4,7% I_N	11,7% I_N
Phase b	1,1% I_N	4,4% I_N	9,6% I_N	23,7% I_N
Phase c	0,7% I_N	2,3% I_N	4,5% I_N	11,9% I_N

B. *Short circuit between non-consecutive turns*

The short-circuit scenario between non-consecutive turns was simulated by introducing a short-circuit resistance between points 7 and 8 for the case of primary winding failure and between points 11 and 12 for the case of secondary winding defect, as we can see in Figure 6. This transformer presents a total of 1700 turns with six conductors in parallel per phase. Simulations were performed with different degrees of short circuit (1%, 2%, 3% and 5% of the number of turns) in order to visualize the impact that the severity of the short circuit will have on the input and output currents and voltages. of the transformer.

1) Primary Side Short-Circuit

Figure 16 and Figure 17 illustrate the evolution of primary and secondary currents, respectively, in the case of a short circuit between three percent of the number of turns of the primary winding.

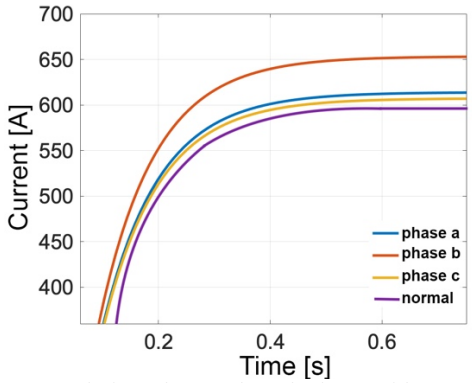

Figure 16 - Evolution of rms value of primary side current

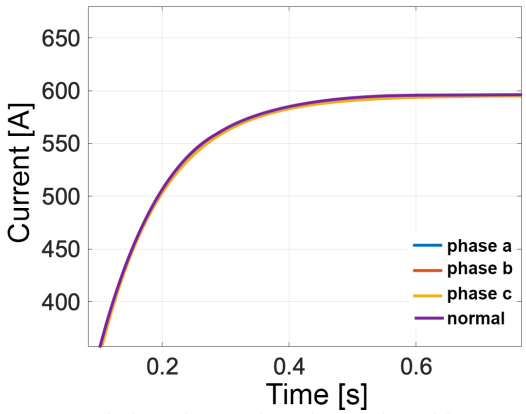

Figure 17 - Evolution of rms value of secondary side current

When compared to the case of short circuit between consecutive turns, there are some differences in the behavior of primary and secondary currents. A short on the primary side causes an increase in current on the primary side, which is more pronounced at the time the fault occurs. However, in the case of a short circuit between consecutive turns, only the fault phase increases, and the other two phases remain within the normal range. In the case of a secondary side currents remain unchanged. This effect is different from what happened in the short circuit between consecutive turns where the value of the secondary currents increased in the fault phase. Comparing the two models, it can be stated that the results are in agreement. Primary currents increase from normal value in both models and secondary currents remain unchanged in both models.

The magnetization current, Figure 18 , results from the sum between the currents of the primary windings and the secondary windings. The method suggested in the previous chapters states that this current should be between 0.1% - 0.3% of the nominal current value

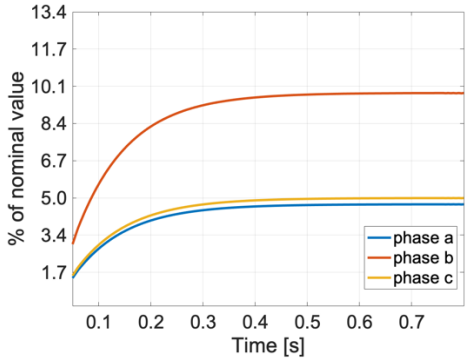

Figure 18 - Evolution of rms value of magnetization current

Analyzing Table 3 shows that with only 1% of the turns short circuit the magnetization current violates the established condition.

It can be concluded that a reduction in the number of turns of the primary winding by one percent with a monitoring of the increase of the input and output currents and the values of the magnetization current exceeding 0.3% of the nominal value leads to the assumption that possibility of a short circuit between turns in the phase where the increase is greatest.

Table 3 - Magnetization currents as a percentage of nominal value

	1%	2%	3%	5%
Phase a	0,4% I_N	2,1% I_N	4,7% I_N	11,9% I_N
Phase b	1,1% I_N	4,4% I_N	9,8% I_N	24,1% I_N
Phase c	0,7% I_N	2,4% I_N	5,0% I_N	12,2% I_N

2) Secondary Side Short-Circuit

Figure 19 and Figure 20 show the primary and secondary currents, respectively, when a short in the secondary winding occurs.

A fault in phase *b* of the secondary winding leads in both analyzes to a reduction in the current from the secondary side and also on the primary side in the phase in which the defect occurs. This is because the number of effective turns in the secondary decreases. As it decreases, the induced secondary voltage decreases and, since the transformer load is a pure resistance, the current corresponding to the phase in which the fault occurs is also reduced. This effect of the current reduction is evident in both models, and in all cases the number of turns reduces agreement between the models. Input voltages do not change from the nominal value.

From the point of view of magnetization currents, it is possible to identify the defect and its phase, even with only 1% of defect, and this effect is similar in both models.

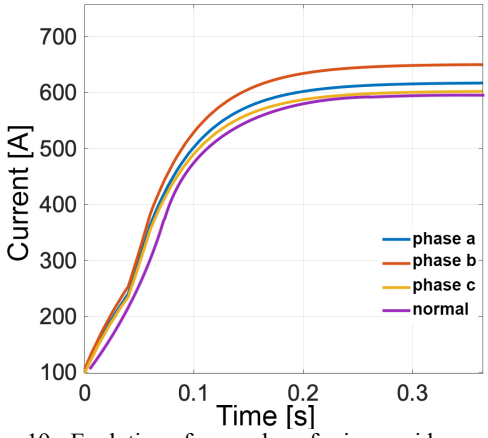

Figure 19 - Evolution of rms value of primary side current

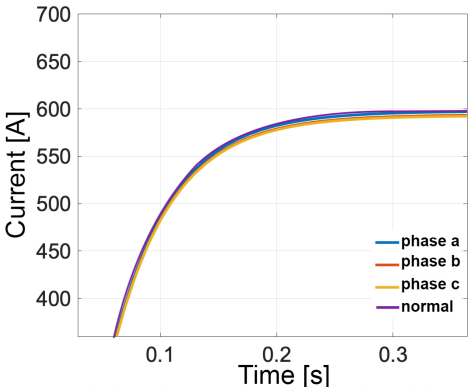

Figure 20 - Evolution of rms value of secondary side current

Once again, the curves of the magnetization current, Figure 21, were plotted to verify the condition studied. Table 4 summarizes the percentage changes, showing that from one percent of the reduction in the number of turns of the secondary winding the magnetization current exceeds 0.3% of the nominal current.

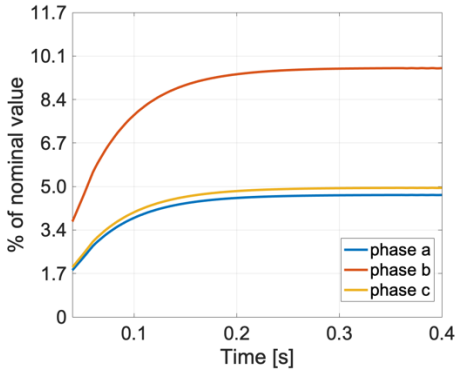

Figure 21 - Evolution of rms value of magnetization current

Table 4 – Magnetization currents as a percentage of nominal value

	1%	2%	3%	5%
Phase a	0,5% I_N	0,8% I_N	1,2% I_N	1,8% I_N
Phase b	0,7% I_N	1,3% I_N	2,6% I_N	3,3% I_N
Phase c	0,2% I_N	0,2% I_N	0,5% I_N	1,5% I_N

3) Aging Insulation Resistance

One of the internal defects of the transformer may be related to the aging of the insulation resistance, and it may be advantageous to perform electrical tests for its characterization. Insulation resistance varies with humidity and temperature and also with the presence of various particles suspended or deposited in the oil in the case of oil transformers. Insulation resistance measurement is a type of test used to measure the insulation quality of each of the windings in relation to ground and between the windings. In order to test the influence of aging of the insulation resistance on the appearance of transformer failures, the defect was simulated. A resistor was placed between the fault phase coil and ground, first on the primary side and then on the secondary side. Consideration was given to this test for the different winding zones along the transformer section (top, middle and bottom). Various insulation resistance values corresponding to 100%, 10%, 1%, 0.1% and 0.01% of the standard insulation resistance were used.

In all cases, the simulation results (Figure 20 and Figure 21) show that there are no significant changes in current as well as voltage compared to the normal operating condition. Therefore, it is concluded that no relevant effects on transformer currents and voltages are observed, regardless of whether the defect is located in the primary or secondary windings. As previously noted, no change in magnetization currents is visible either.

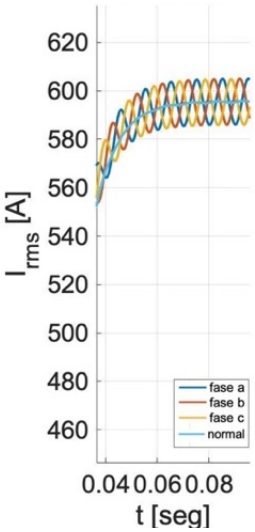

Figure 20 - Evolution of rms value of primary side current

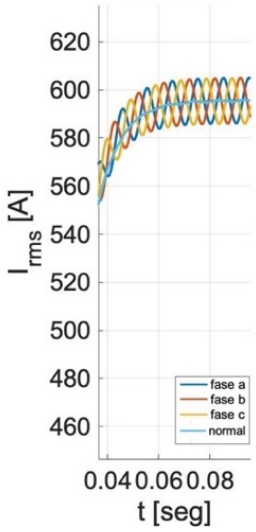

Figure 21 - Evolution of rms value of secondary side current

Figure 22 represents the leakage currents for the various simulated resistance values. The values of leakage currents are found to be small, tending to zero with increasing insulation resistance. However, the values of these currents are high enough to be detected by a differential protection.

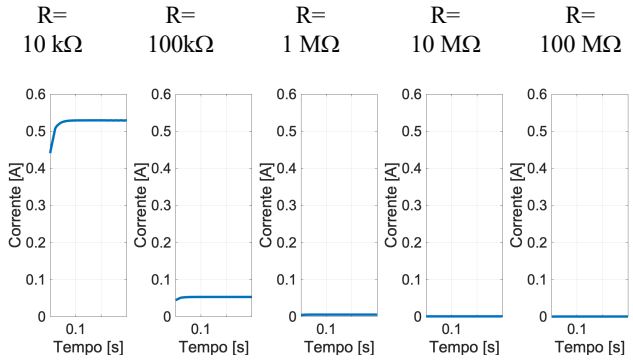

Figure 22 – Leakage Currents

C. Profile of Each Fault

The application of finite element methods as well as analytical methods had as main objective the creation of a model for simulation of failures between turns of a transformer. With these it was possible to distinguish profiles of current and voltage behaviors that occur during a failure. The incidence of shorting the primary or secondary winding between consecutive turns presents concordant results in both models. In a short circuit between non-consecutive turns, agreement of the results is also verified whether the short circuit is in the primary or secondary winding.

Since the results in the general case show agreement, it is possible to define profiles to identify the short circuits in the windings:

Profile A: The occurrence of an increase in current in the primary and secondary side defect phase, accompanied by the inalterability of the remaining phases, identifies a short circuit in the primary winding between consecutive turns.

Profile B: The occurrence of a decrease in the input and output current, this increase being more pronounced in the fault phase, allows the recognition of a short circuit in the secondary winding between consecutive turns.

Profile C: an increase in currents in phases a and c, accompanied by a marked increase in the fault phase current in the primary winding, and the secondary side currents do not show significant changes allowing to identify a short circuit between consecutive turns. However, it is not possible to identify which winding is defective, as the phase variations are similar to each other.

IV. CONCLUSIONS

In this work we review the main types of faults and diagnostic methodologies used for fault detection in power transformers. The methods chosen for fault detection without removing the transformer from operation are checking the magnetization currents and the transformer leakage currents. The first focuses on the magnetization current analysis which, based on the literature review, should be around 0.1% -0.3% of the nominal current for normal transformer operation. The other method focuses on the analysis of leakage currents in order to trace alarm indicators for the preventive detection of insulation aging.

Two models have been developed, one analytical and the other in finite element (FEM) so that fault diagnosis is more reliable and robust. The analytical model is based on the combined analysis of transformer equivalent magnetic and electrical circuits. The FEM model is based on the division of the problem into homogeneous subdomains and provides more accurate solutions to complex problems at the expense of longer processing times.

The developed models are validated (section 4) in simulation. In the identification of short circuits between consecutive turns, as well as in the identification of short circuits between non-consecutive turns, the results are in agreement with each other. From the results acquired by the short circuits, it was possible to create profiles that could preventively identify the fault situation in which it may be. The calculation of the magnetization current allows the preventive detection of transformer turns between defects, even in the case of 1% short circuit. In the case of the resistance aging simulation it was found that only with a large variation of the insulation resistance the leakage currents tend to non-normal values.

V. REFERENCES

Fofana, I. (2018). *"Power Transformer Diagnostics, Monitoring and Design Features".*